

# Triarylamines as Catholytes in Aqueous Organic Redox Flow Batteries

Nadia L. Farag,<sup>[a]</sup> Rajesh B. Jethwa,<sup>[b]</sup> Alice E. Beardmore,<sup>[a]</sup> Teresa Insinna,<sup>[a]</sup> Christopher A. O'Keefe,<sup>[a]</sup> Peter A. A. Klusener,<sup>[c]</sup> Clare P. Grey,<sup>\*[a]</sup> and Dominic S. Wright<sup>\*[a]</sup>

A series of triarylamines was synthesised and screened for their suitability as catholytes in redox flow batteries using cyclic voltammetry (CV). Tris(4-aminophenyl)amine was found to be the strongest candidate. Solubility and initial electrochemical performance were promising; however, polymerisation was observed during electrochemical cycling leading to rapid capacity fade prescribed to a loss of accessible active material and the limitation of ion transport processes within the cell. A mixed electrolyte system of H<sub>3</sub>PO<sub>4</sub> and HCl was found to inhibit

polymerisation producing oligomers that consumed less active material reducing rates of degradation in the redox flow battery. Under these conditions Coulombic efficiency improved by over 4%, the maximum number of cycles more than quadrupled and an additional theoretical capacity of 20% was accessed. This paper is, to our knowledge, the first example of triarylamines as catholytes in all-aqueous redox flow batteries and emphasises the impact supporting electrolytes can have on electrochemical performance.

## Introduction

To combat the effects of the climate crisis, the world must switch to renewable energy sources, such as wind or solar power. However, due to the unpredictability of weather conditions, storage and smooth distribution of energy from these sources is crucial. Li-ion batteries (LIBs) are currently the most well-developed energy storage system, but the limited cost and sustainability of lithium and cathode materials (Co and Ni in particular) are a current and future concern. Therefore, an alternative technology to LIBs is required for large scale electrical grid applications. Redox flow batteries (RFBs) are a promising candidate system for grid-level electrical storage, using some design principles from both fuel cells and batteries, with some distinct advantages.<sup>[1,2]</sup> The most notable feature of RFBs is the decoupling of capacity and power, allowing them to be scaled separately.<sup>[3]</sup> This decoupling allows flexible battery performance across a range of applications and time-scales.<sup>[2]</sup>

Currently, the most developed RFB electrolyte system is based on vanadium; however, vanadium is an expensive and toxic metal that has a limited energy density (owing to solubility limitations).<sup>[3–5]</sup> With this in mind, there has been an increased focus on organic electrolytes that are soluble under aqueous conditions [so-called aqueous organic RFBs (AORFBs)]. However, it must be noted that aqueous solvent systems suffer from a smaller potential window than organic solvent systems due to water splitting, and therefore achieving high voltage batteries is difficult. The target solubility for organic electrolytes in aqueous RFBs for a commercially viable system is 2 M, but the vast majority of currently explored organic electrolytes struggle to meet this.<sup>[6]</sup> This balance between solubility and stability is a difficult tightrope to traverse, especially since the mere introduction of a solubilising functionality onto the anolyte or catholyte framework can result in decreased cycling stability or complete loss of electrochemical activity.<sup>[7–9]</sup> Nonetheless, the overall advantages of safety (due to the aqueous electrolyte), cost, and fast kinetics make the development of aqueous organic RFBs (AORFBs) an important area of study.


Importantly, although there has been considerable development of organic aqueous-soluble anolytes for RFBs, there are comparatively few catholytes of this type.<sup>[10]</sup> While motifs such as TEMPO (2,2,6,6-tetramethylpiperidine-1-oxyl), ferrocene and ferrocyanide have all been explored as catholytes in AORFBs, none of these currently meet the performance thresholds needed for commercial systems and problems such as capacity fade and low solubility continue to plague the field.<sup>[3,11,12]</sup> The US Department of Energy has set a solubility target of 2 M for an organic-aqueous RFB, a value which has yet to be met.<sup>[6]</sup>


In order to develop a fully organic aqueous flow battery system (containing a catholyte and anolyte which are both organic molecules), it is imperative to introduce new classes of organic catholytes with the solubility, stability and energy density required for commercial viability.

[a] N. L. Farag, A. E. Beardmore, T. Insinna, Dr. C. A. O'Keefe, Prof. C. P. Grey, Prof. D. S. Wright  
 Department of Chemistry, Yusuf Hamied Department of Chemistry  
 University of Cambridge  
 Lensfield Rd, Cambridge, CB2 1EW (United Kingdom)  
 E-mail: cpg27@cam.ac.uk  
 dsw1000@cam.ac.uk

[b] Dr. R. B. Jethwa  
 Institute of Science and Technology  
 Am Campus 1, Klosterneuberg, 3400 (Austria)

[c] Dr. P. A. A. Klusener  
 Shell Global Solutions International B.V.  
 Energy Transition Campus Amsterdam  
 Grasweg 31, 1031 HW Amsterdam (The Netherlands)

 Supporting information for this article is available on the WWW under <https://doi.org/10.1002/cssc.202300128>

 © 2023 The Authors. ChemSusChem published by Wiley-VCH GmbH. This is an open access article under the terms of the Creative Commons Attribution License, which permits use, distribution and reproduction in any medium, provided the original work is properly cited.

In addition to the organic redox couple, electrolyte conditions have been shown to have a significant effect on electrolyte behaviour. Work by Milshtein *et al.* and Orita *et al.*, respectively, has shown that minor variations in conditions such as the supporting electrolyte salt used and pH can have significant effects on solubility and electrochemical activity in a RFB.<sup>[13,14]</sup> Additionally, some mixed electrolyte systems and their impact on electrochemical performance have been explored, such as the work by Zhang *et al.*<sup>[15]</sup> Despite this, supporting electrolyte conditions remain an underexplored aspect of electrolyte design for AORFBs.

Triarylamines (TAAs) are a class of molecules with many desirable attributes for redox flow applications such as, ease of functional group modification (allowing variation in their redox potential and solubility), and low reorganisation energy (when transitioning from the neutral to radical geometries).<sup>[16]</sup> Due to a prominent degradation pathway resulting in C–C bond formation and dimerization of the reduced form, substitution of the *para*-position is important for the development of new catholytes based on TAAs (Figure 1a).<sup>[16]</sup> While there are known examples of TAAs which show reversible redox behaviour in non-aqueous solvents at positive potentials, TAAs have primarily been used in photovoltaic applications and have not been greatly explored for aqueous organic RFB applications.<sup>[17]</sup>

Romadina *et al.* demonstrated a non-aqueous organic RFB using a series of TAAs as catholytes. Their study focused on 4-bromo- and 4-diethylene glycol (PEG)-substituted TAAs (Figure 1b) and found the compounds to be highly soluble in acetonitrile with Coulombic efficiencies (CE) over 80%.<sup>[18]</sup> Addi-

tionally, Kwon *et al.* recently published another example of a non-aqueous organic RFB catholyte based on a TAA. Methoxy groups substituted in the *para*-position greatly enhanced the stability in the charged state (Figure 1c).<sup>[19]</sup> While both of these examples focus on non-aqueous catholytes, they demonstrate the promise of TAA-based materials for RFB applications. Finally, Wang *et al.* demonstrated the application of 4,4',4''-trihydroxyphenylamine in a mixed electrolyte system of DMF and H<sub>2</sub>O (1:5 volume ratio).<sup>[20]</sup>

Here we explore the applications of TAAs in aqueous organic RFBs, by synthesising a range of TAA derivatives and testing their redox properties under aqueous conditions. Using cyclic voltammetry (CV), the strongest candidate 4-amino-trisphenyl amine (**1**) was identified for battery testing, although poor cycling stability was identified as an issue due to the formation of a polymer film at the working electrode. The supporting electrolyte was optimised to maximise the solubility of **1** while minimising its degradation due to undesirable polymerisation at the catholyte electrode. This work highlights the importance of the supporting electrolyte system in preventing degradation of TAAs in AORFBs and as well as in the general field of catholyte development in this area.

## Results and Discussion

### Synthesis and initial electrochemical testing

To investigate the aqueous electrochemistry and battery performance of molecules based on the TAA framework, a series of candidates was synthesised with an initial emphasis on aqueous solubility (Figure 1d), utilising amine and carboxylic acid groups at their 4-positions to prevent C–C bond formation during cycling. All candidates were synthesised via an aromatic substitution reaction detailed in the Supporting Information. It was found that the combination of these groups in the *para*-positions of the three phenyl rings greatly impacted both the solubility and electrochemistry. The tris-amino- compound **1** was found to have a reversible redox process at 0.75 V vs standard hydrogen electrode (SHE) in acidic conditions (Figure 2) while replacing one of the –NH<sub>2</sub> groups with –CO<sub>2</sub>H in **2** produced some quasi-reversible processes (Figure S4). However, based on the peak-to-peak separation which greatly exceeded 57 mV indicating this was not a reversible process, **2** was ruled out as a catholyte candidate. Compounds **3**, **4** and **5** lacked any reversible redox activity (Figure S5 to Figure S7), though all were soluble under acidic conditions. **3** was found to be soluble under acidic, neutral, and basic aqueous conditions. This was ascribed to the potential formation of a zwitterion, i.e., the ability to form an –NH<sub>3</sub><sup>+</sup> and –CO<sub>2</sub><sup>–</sup> tautomer in solution. Based on the initial electrochemical survey of compounds **1**–**5**, the addition of –CO<sub>2</sub>H electron withdrawing groups destabilised the charged state, resulting in irreversible redox behaviour, while the electron donating NH<sub>2</sub> groups had the opposite effect, stabilising charged states through additional, favourable, delocalisation. There is evidently a balance to this effect as the more strongly electron donating N–Me<sub>2</sub> groups in compound **4**

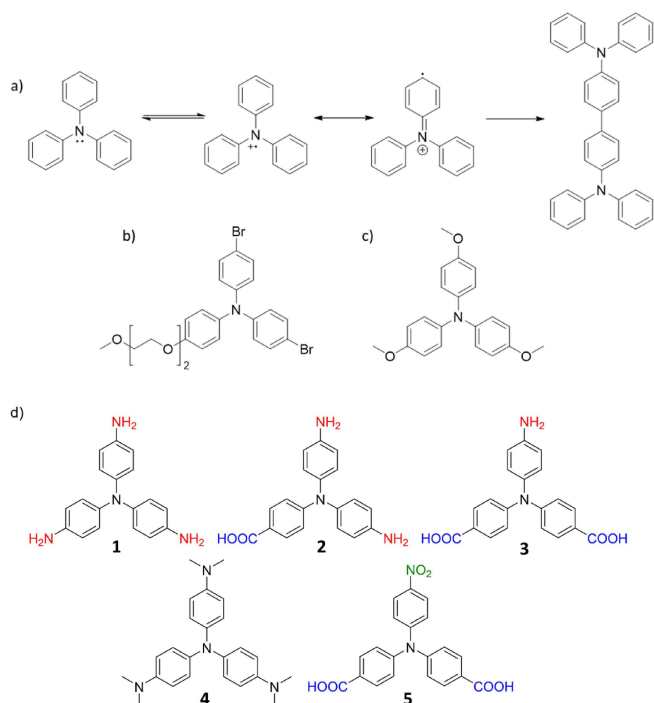


**Figure 1.** a) Redox process associated with TAA and the subsequent degradation experienced via the unoccupied *para* position. b) The compound explored by Romadina *et al.*<sup>[18]</sup> c) The compound explored by Kwon *et al.*<sup>[19]</sup> d) The series of TAA compounds investigated in the current study.

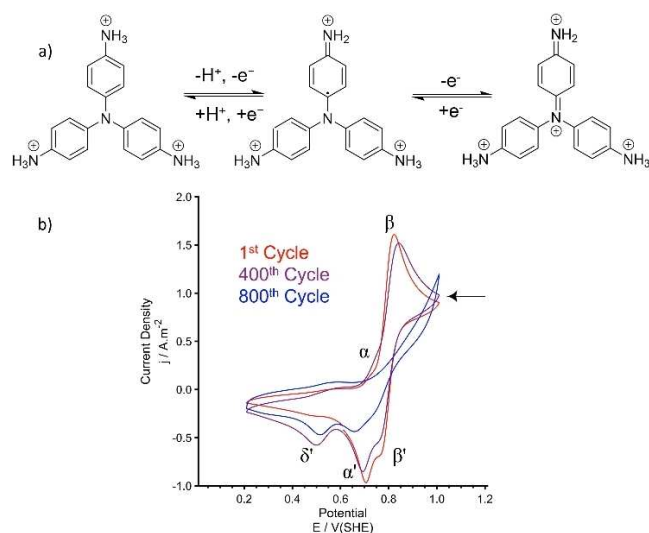


**Figure 2.** Initial screening of compound 1. a) Predicted two  $1 e^-$  transfer processes. b) CV of  $1 \text{ mM}$  **1** in  $1 \text{ M HCl}$ , with a glassy carbon working electrode (GCWE), Ag/AgCl reference electrode and Pt counter electrode. The CV was measured at  $25^\circ\text{C}$  under an inert  $\text{N}_2$  atmosphere.  $\alpha$  and  $\beta$  are the two oxidation processes, with  $\alpha'$  and  $\beta'$  being the corresponding reductive peaks,  $\delta'$  is a partially irreversible reduction peak which grows in over the course of cycling.

were found to undergo only semi-reversible redox, with a stronger preference for oxidation (Figure S6). Only compound **1** was selected for further electrochemical investigation, on the basis of its electrochemical behaviour and solubility. Compound **1** has many desirable properties for RFB applications including facile synthesis and the potential for the amine groups to enhance aqueous solubility through hydrogen bonding and protonation under acidic conditions.

**1** was found to be soluble up to  $350 \text{ mM}$  in  $1 \text{ M HCl}_{(\text{aq})}$  (pH0). The competitive solubility of **1** under acidic conditions is clearly the result of protonation of some or all of the  $-\text{NH}_2$  groups, resulting in an increase in charge of the molecule in solution. This solubility, however, decreased rapidly with increasing pH, with (e.g.) a maximum solubility of  $5 \text{ mM}$  at pH2 ( $10 \text{ mM HCl}$ ).

Two redox processes are seen for **1** in  $1 \text{ M HCl}_{(\text{aq})}$  at approximately  $0.75 \text{ V}$  vs SHE at  $1 \text{ mM}$  concentration ( $\alpha/\alpha'$  and  $\beta/\beta'$ , Figure 2) with peak-to-peak separations between the oxidation and reduction waves of ca.  $50 \text{ mV}$ , indicating that these are most likely two  $1 e^-$  transfer processes, with overlap of the peaks for the two processes, particularly on charging, giving the appearance of one process. The most likely electrochemical processes responsible for this behaviour are the successive  $1 e^-$  oxidations of **1** (Figure 2a). A largely irreversible reduction peak at  $0.5 \text{ V}$  vs SHE was also seen to grow gradually over the course of cycling ( $\delta'$  in Figure 2) Before 800 cycles, the reversible electrochemical processes at  $0.75 \text{ V}$  vs SHE were lost. This occurred even if the CV experiment was undertaken in the dark, indicating that there is no major contribution from photochemical degradation and that the evolution of the electrochemistry is due to the intrinsic degradation of **1** itself.

Analysis of the solution by  $^1\text{H NMR}$  spectroscopy after the 800 CV cycles showed no apparent degradation of **1** (Figure S10), however, due to the low concentration of the CV sample ( $1 \text{ mM}$ ) there may conceivably be trace degradation products which could not be detected. Electrochemical impedance spectroscopy (EIS) measurements strongly suggest that a major product of the observed degradation of **1** with cycling is the formation of a film on the working electrode (WE); there is an observable difference in the impedance measured before and after 800 CV cycles (Figure 3), reflecting a change in the electron-transfer resistance.

Polishing the WE after a period of cycling of solutions of **1** resulted in recovery of the initial electrochemistry, further supporting the view that the degradation of **1** to form a film on the WE is a major contribution to the overall capacity fade (Figure 4, b and c). This does not exclude the possibility of degradation processes in solution, some of which may be associated with the formation of the film, and we suspect that the irreversible reduction peak at  $0.5 \text{ V}$  vs SHE,  $\delta'$ , that becomes apparent on prolonged cycling is associated with solution intermediates involved in the formation of the insoluble film. To confirm this, CV was run of a fresh electrolyte using a reduced voltage window of  $0.6\text{--}1.0 \text{ V}$  vs SHE, therefore excluding process  $\delta'$ . This resulted in increased in cycling stability as shown in Figure 4d, but the gradual loss of current density over time indicated that further degradation pathways are also occurring (probably in solution).

Full-cell RFBs were run initially using **1** as the catholyte at  $100 \text{ mM}$  concentration, charging to  $1.9 \text{ V}$  at  $10 \text{ mA cm}^{-2}$  against an excess of  $\text{VCl}_2/\text{VCl}_3$  anolyte. A large voltage window of  $1.7 \text{ V}$  ( $0.2$  to  $1.9 \text{ V}$ ), exceeding the stable cycling window for water, was used initially to explore any processes occurring at high voltages. This was reduced to a  $1.3 \text{ V}$  window ( $0.2$  to  $1.5 \text{ V}$ ) in subsequent studies (see later). The low charging current employed reflects the slow redox kinetics of the system, which was established through rotating disk measurements (Figure S11). Figure 5a shows the first charge cycle where a two-step oxidation which greatly exceeds the theoretical capacity is observed. Subsequent cycles demonstrated dramatic capacity loss and negligible capacity beyond 10 cycles. A black polymer

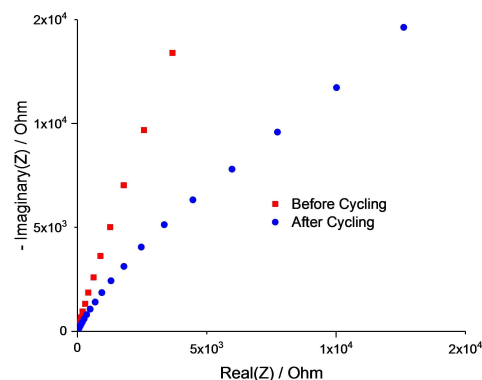


**Figure 3.** Impedance measured before and after CV was run on compound **1** (800 cycles).

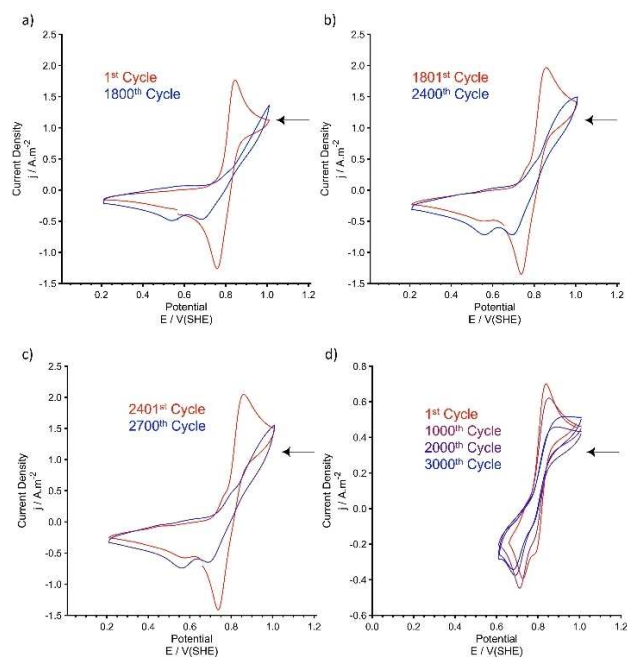


**Figure 4.** a) First 1800 cycles of CV which was run until reversible electrochemistry was lost (full cycling can be seen in Figure S8); the CV was run with 1 mM **1** in 1 M HCl, using a Pt counter electrode, Ag/AgCl reference electrode and GCWE. b) First cycle taken after polishing the WE (1801) and the last cycle measured before reversible redox was completely lost (600 cycles). c) First cycle taken after polishing the WE (2401) and the last cycle measured before reversible redox was completely lost (300 cycles). d) CV of a fresh solution with a reduced cycling window from 0.6 to 1.0 V vs SHE, demonstrating up to 3000 cycles.

had formed during cycling and was discovered during cell disassembly. Due to the convective motion of RFB electrolytes, it is difficult to ascertain exactly where polymerisation was initiated but based on the large capacity observed during the first cycle, it most likely occurs at the electrode. Attempts to combat this capacity fade involved reducing the voltage to 1.5 V (Figure 5b) and varying the concentration of **1** between 33–300 mM (Figure S13). Unfortunately, polymerisation was found to occur under all these conditions. Although the rate of polymerisation was reduced at lower concentrations, the capacity loss was still significant, with a maximum capacity of just over 0.6 AhL<sup>-1</sup> when using a 33 mM solution of **1** (compared to a maximum of over 2.5 AhL<sup>-1</sup> with a 300 mM solution). In all battery runs, the first charge cycle demonstrated unique behaviour compared to the subsequent cycles which exhibited two charge plateaus (in agreement with the predicted mechanism deduced from the  $\alpha/\alpha'$  and  $\beta/\beta'$  redox couples seen in CV, Figure 2a).

Triarylamines are known to undergo polymerisation, indeed they are often used as precursors for thin-film polymer formation.<sup>[21,22]</sup> It is therefore reasonable to assume that the film formed in these experiments results from the polymerisation of **1**. In 2010, Moulin *et al.* found that by simply exposing a number of triarylamine species to light it was possible to generate triarylammonium radicals, with the radical localised to the central nitrogen, these radicals were found to undergo self-assembly resulting in larger, aggregated structures.<sup>[21,23]</sup> On the basis of this previous work, our hypothesis is that during cycling of **1**, unstable nitrene radicals could be produced during the initial oxidation; subsequent polymerisation being driven by the chemical reactions between these radicals. An extended net-

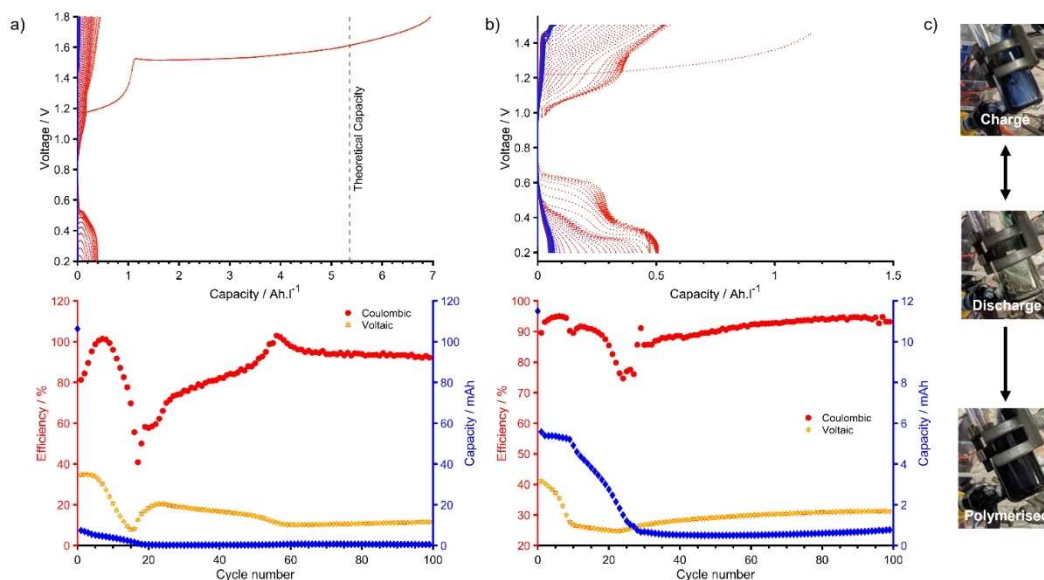


**Figure 5.** Galvanostatic cycling data for 100 mM **1** in 1 M HCl, with a VCl<sub>2</sub>/VCl<sub>3</sub> anolyte (150 mM) over 100 cycles on top, while the bottom half plots CE (red), voltaic efficiency (orange) and capacity (blue) against cycle number. a) Charging to 1.9 V, and b) charging to 1.5 V. c) Images of the catholyte solution during charge and discharge of the first few cycles, before polymerisation turns the solution black (within the first five cycles).

work would then be formed which aggregates further, driven by  $\pi$ -bonding interactions between the polymer sheets.

The nature of the radical present, both in the monomer and polymer, was investigated using electron paramagnetic resonance (EPR) and NMR spectroscopy, while the composition of the polymer was assessed with gel permeation chromatography, mass spectrometry (MS), elemental analysis and IR spectroscopy, results of which can be seen in the Supporting Information (Table S2, Figure S18 to Figure S21). While the exact nature of the polymer could not be determined, these studies did confirm an extended bonding network, loss of nitrogen from the system and from the MS, a possible repeat unit with an  $m/z$  of 224 was identified. Additionally, the  $^{13}\text{C}$  solid-state NMR spectrum (Figure S20) of the polymer shows peaks between 85 and 95 ppm, which are outside of the chemical shift range expected for  $\text{sp}^2$  carbons suggesting the presence of non-aromatic carbons atoms.

*Ex situ* solution EPR measurements were performed on **1** in the oxidised state (Figure 6). The catholyte was charged to 1.5 V, an aliquot of the solution was taken, and a sample was prepared for EPR (all under inert atmosphere). A spectrum was taken of this sample every ten minutes over the course of two days to assess how the radical changed over time. Over the course of the two days, the EPR spectrum evolved, indicating a change in the structure of the radical in solution. Suspected radical environments, **R1**, **R2** and **R3** can be seen in Figure 6c.

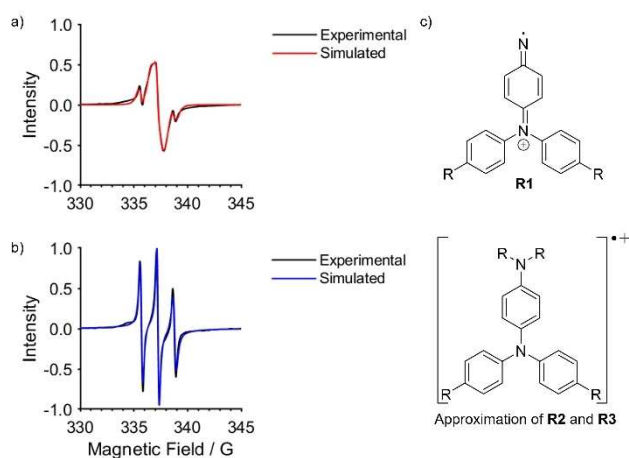


**Figure 6.** Radicals were modelled using a  $^{14}\text{N}$  nucleus using the fitting parameters outlined in Table 1. EPR spectra measured for (a) a freshly charged sample (red), and (b) the sample after 48 h, stored in the dark under an inert atmosphere (blue). c) Proposed radical structures for **R1**, **R2** and **R3**.

**R2** and **R3** are believed to be similar radical environments with radical cations occupying either a central or terminal nitrogen but as no strong conclusions can be drawn regarding the exact structures they have been depicted as seen in Figure 6c. The radicals have been assigned based on the hyperfine coupling constants obtained from fitting said resonances (Table 1). Applying McConnell's relation to our aromatic system results in two forms of spin polarisation, one originating from a  $\pi$ - $\sigma$  polarisation (with  $a < 0$ ) and one originating from a  $\pi$ - $\pi$  polarisation (with  $a > 0$ ).<sup>[24]</sup>  $\text{sp}^2$  interactions must therefore lead to positive hyperfine values, and hence **R1** was assumed to have all positive hyperfine coupling values while **R2/R3** have a mix of positive and negative values. While there are small differences in the hyperfine coupling values used to fit the fresh and aged samples, these are within error (approximately 10%), and so they can be assumed to be the same radical environments.

By comparing the relative weights of the different radical environments, it can be seen that **R1** only makes up 0.42% of the initial radical species with this value increasing to 22.61% over the course of the two days. Possibly this is an indication of the termination product within the system resembling **R1**, which may form on the end of polymer chains. The radical cations (**R2/R3**) can be assumed to be the initial radical products formed during cycling and are likely to react with amino groups as well as with the aromatic rings to form the polymer over time. This polymerisation will limit the tumbling speed in solution, likely explaining the broad line shapes observed (and the long correlation times obtained in the fit) and asymmetric nature of the EPR peaks. These features can also be accounted for by the multiple radical signals which are overlapping. Additionally, the decrease of **R2** over time from 56.18% to 1.95% suggests that this is the more reactive of the two radical cation species. The major radical species identified after long-term cycling was found to persist after long-term exposure to ambient light in air, with exposed samples continuing to demonstrate radical activity after the same 48 h under these conditions.

### Reducing polymerisation through $\text{H}_3\text{PO}_4$ in the supporting electrolyte

To make this system viable for RFB applications, excluding or slowing down the formation of the polymer is essential.  $\text{H}_3\text{PO}_4$  was chosen to replace HCl as the supporting electrolyte as

**Table 1.** Details of the radical environments as modelled in a fresh and aged sample.

Radical	<b>R1</b> <sup>[a]</sup>	<b>R2</b> <sup>[b]</sup>	<b>R3</b> <sup>[b]</sup>
<i>g</i> Value	2.0088, 2.0061, 2.0027	2.0053	2.0058
Log10 of rotational correlation time	-8.00	-8.05	-7.67
Hyperfine coupling constant (Figure 6a)	49.0, 29.6, 50.9	-1.1, -19.4, 29.4	-19.4, -11.3, 54.2
Relative weights (Figure 6a)	0.42%	56.18%	43.40%
Hyperfine coupling constant (Figure 6b)	47.5, 30.7, 51.6	-2.1, -18.6, 29.4	-19.4, -13.1, 55.4
Relative weights (Figure 6b)	22.61%	1.95%	75.44%

[a]  $\text{sp}^2$  delocalisation. [b]  $\text{sp}$  delocalisation.

Schlemmer et al. have previously demonstrated that its use could stabilise organic radicals such as 2-methoxyhydroquinone (leading to longer radical lifetimes and reduced reactivity of radicals) and mitigate their degradation.<sup>[25]</sup> While the reasons for this stabilisation are still debated, it is likely that strong hydrogen bonding interactions stabilise reactive radical intermediates, reducing their rate of degradation and/or polymerisation (Figure 7).<sup>[25–27]</sup>

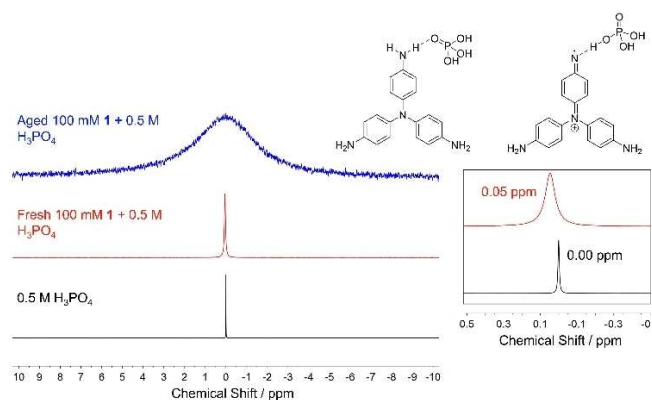


**Figure 7.**  $^{31}\text{P}$  NMR spectra showing the phosphoric acid peak of  $0.5\text{ M H}_3\text{PO}_4$  (black; bottom), a fresh sample of  $100\text{ mM } 1$  in  $0.5\text{ M H}_3\text{PO}_4$  (red) and an aged sample of  $100\text{ mM } 1$  in  $0.5\text{ M H}_3\text{PO}_4$  (blue; top). The chemical shifts of the isotropic resonances are marked. Predicted H-bonding interactions with  $1$  and the nitrene radical thought to be involved in the polymerisation process as shown above.

To investigate this,  $^{31}\text{P}$  NMR spectra were run on three different samples: fresh  $0.5\text{ M H}_3\text{PO}_4$ , fresh  $0.5\text{ M H}_3\text{PO}_4$  with  $100\text{ mM } 1$ , and an aged sample of the same composition ( $0.5\text{ M H}_3\text{PO}_4$  with  $100\text{ mM } 1$ ) which had been left for a week in an inert atmosphere but with light exposure (Figure 7). A small shift in the  $^{31}\text{P}$  phosphoric acid resonance was observed upon the addition of  $1$ , as well as peak broadening in the aged sample the latter suggesting the presence of paramagnetic species. The observed change in chemical shift upon addition of  $1$  is indicative of an interaction between  $1$  and phosphoric acid; however, because the shift was small,  $^{31}\text{P}$  spin-lattice relaxation time constants ( $T_1$ ) were measured to explore these interactions further. Strong hydrogen-bonding of  $\text{H}_3\text{PO}_4$  molecules to  $1$  should result in a complex with a longer rotational correlation time, if there is a long-lived complex and there are no relaxation effects due to radicals and therefore this difference should be reflected in the values of the  $^{31}\text{P } T_1$ . The  $T_1$  values were found to change from  $17.14\text{ s}$  for  $0.5\text{ M H}_3\text{PO}_4$  to  $1.42\text{ s}$  a freshly prepared solution of  $100\text{ mM } 1$  in  $0.5\text{ M H}_3\text{PO}_4$  (Figure S1). The change in viscosity between the two samples was minimal (kinematic viscosity was  $1.12$  and  $1.26\text{ cSt}$ , respectively), dynamic viscosity was  $1.30$  and  $1.50\text{ cP}$ , respectively), thus confirming that the significant change in  $T_1$  is likely due to interactions between  $1$  and  $\text{H}_3\text{PO}_4$  affecting the tumbling rate of the phosphate group.

An initial electrochemical investigation using  $\text{H}_3\text{PO}_4$  as the supporting electrolyte yielded promising results, with longer-term CV cycling indicating increased stability (Figure 8). A lab-

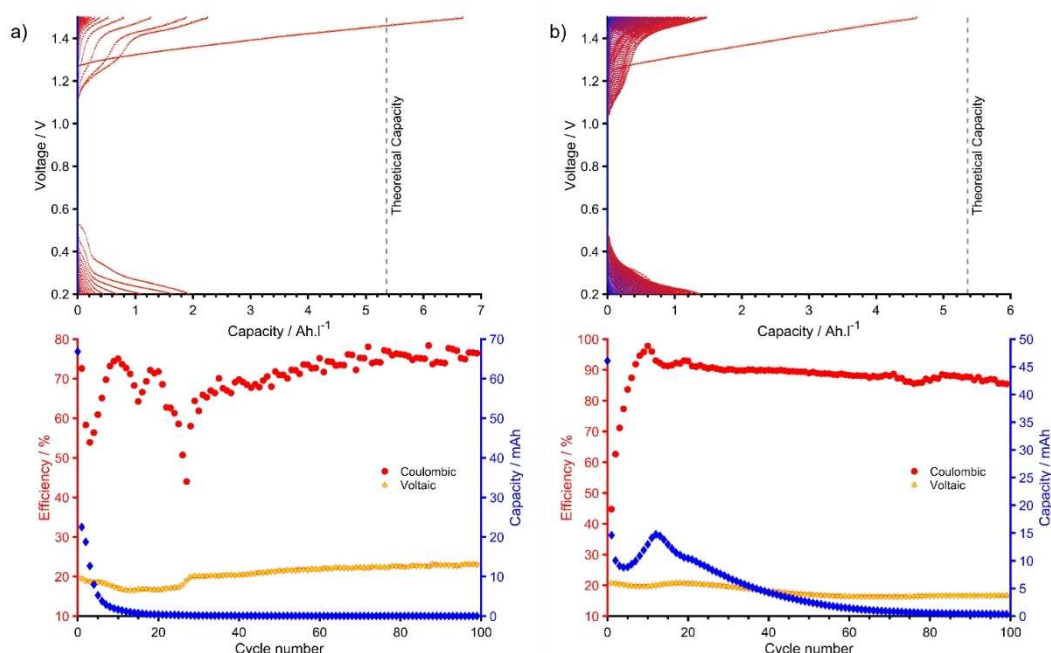


**Figure 8.** Galvanostatic cycling data, charging to  $1.5\text{ V}$  of  $\text{H}_3\text{PO}_4$  electrolyte with a  $\text{VCl}_2/\text{VCl}_3$  ( $120\text{ mM}/30\text{ mM}$ ) anolyte over 100 cycles on top, while the bottom half depicts CE (red), capacity (blue) and VE (orange) against cycle number; a)  $100\text{ mM}$  of  $1$  in  $1\text{ M H}_3\text{PO}_4$  over 100 cycles and b)  $100\text{ mM}$  of  $1$  in  $0.5\text{ M H}_3\text{PO}_4$  over 100 cycles.

scale RFB was then run using 100 mM of **1** in 1 M H<sub>3</sub>PO<sub>4</sub> as the catholyte and VCl<sub>2</sub>/VCl<sub>3</sub> in 1 M H<sub>3</sub>PO<sub>4</sub> for the anolyte. The initial H<sub>3</sub>PO<sub>4</sub> concentration used was 1 M; however, it was found that 0.5 M resulted in both a better CE and better capacity retention for the RFB (Figure 8). Though it still failed to reach the theoretical capacity of 53.53 mAh L<sup>-1</sup>, this can likely be attributed to the lower voltage cut off (necessary due to high rates of polymerisation beyond 1.5 V) and polymerisation removing active material from solution. Similar observations were made by Schlemmer et al. in regard to the concentration-dependence of radical stabilisation.<sup>[25]</sup> By comparing impedance measurements before and after cycling (Figure 9), a relationship between battery performance and resistance after cycling was identified: comparing the resistance values at the electrodes,  $R_2$  and  $R_3$ , between the three different supporting electrolytes, the highest resistance (40.64 Ω) was observed in the 1 M H<sub>3</sub>PO<sub>4</sub> electrolyte, corresponding to the worst overall battery performance (see Table 1). Note that  $R_1$  represents ohmic resistance of the system, and because there is not a significant difference across the three values (0.31, 0.01 and 0.34 Ω for 0.5 M H<sub>3</sub>PO<sub>4</sub>, 1 M HCl and 1 M H<sub>3</sub>PO<sub>4</sub> respectively), no reliable conclusions can be inferred from the  $R_1$  values.

In 0.5 M H<sub>3</sub>PO<sub>4</sub>, the capacity was observed to increase for a few cycles after the initial capacity loss associated with the first

cycle. This suggests that there are at least two degradation processes taking place. Wetting of the electrode could also result in this behaviour. Changing the electrolyte may impact the rate of wetting of the electrodes, resulting from an increase in active area and improved electron transfer kinetics if the wetting improves within the first few cycles (i.e., the electrode, initially, was not fully wetted). However, over time, the capacity continues to decay as the polymer aggregates at, or within, the membrane, inhibiting charge-balancing ion motion. A similar rise and fall are observed in the CE from the 1 M H<sub>3</sub>PO<sub>4</sub> cell (Figure 8), however this is not reflected in the capacity in this case. Table 2 compares the battery performance metrics for the number of cycles in each battery where the capacity is not negligible (negligible was considered to be below 2 mAh). This highlights the differences across the three supporting electrolytes, especially the improvement between 1.0 M and 0.5 M H<sub>3</sub>PO<sub>4</sub>. It can be noted that the experimental capacity exceeds 100% of the theoretical in cycle 1 (for 1 M H<sub>3</sub>PO<sub>4</sub> supporting electrolyte). We tentatively suggest that this is due to polymerisation of the catholyte which produces more redox-active species. These are then electrochemically oxidised, leading to a higher concentration of electrochemically active materials and to an initial capacity exceeding 100% of the theoretically calculated value.

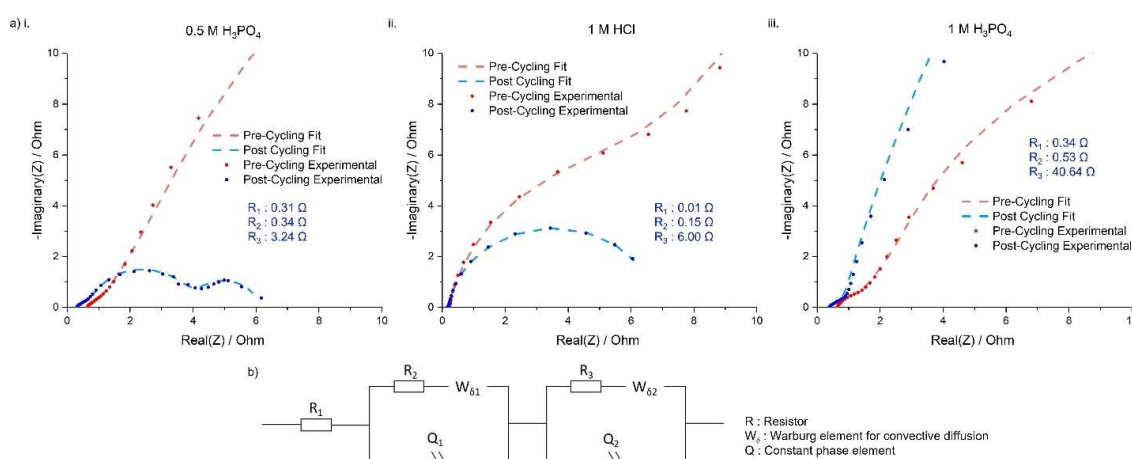


**Figure 9.** a) Impedance taken before galvanostatic battery cycling (conditions as described above) and after 100 cycles with 100 mM **1** in i) 0.5 M H<sub>3</sub>PO<sub>4</sub> electrolyte, ii) 1 M HCl electrolyte and iii) 1 M H<sub>3</sub>PO<sub>4</sub> electrolyte. b) The circuit used to model impedance based on work by Li et al.<sup>[28]</sup>  $R_1$  represents the Ohmic resistance, while  $R_2$  and  $R_3$  represent the interfacial resistances at each electrode. All post cycling impedance was plotted up to an x axis value of 6 Ω to allow for comparable resistance values.

Elec.	Cycle stability	ACap 1 <sup>st</sup> cycle [%]	ACap 2 <sup>nd</sup> cycle [%]	CE [%]	VE [%]	EE [%]
1 M HCl	16	21.48	10.41	92.30 ± 0.51	31.58 ± 1.51	29.21 ± 1.41
1 M H <sub>3</sub> PO <sub>4</sub>	9	124.89	42.09	65.96 ± 2.62	18.49 ± 0.21	11.99 ± 0.50
0.5 M H <sub>3</sub> PO <sub>4</sub>	55	85.98	27.28	88.71 ± 1.08	19.15 ± 0.18	16.98 ± 0.26
0.5 M H <sub>3</sub> PO <sub>4</sub> + 0.5 M HCl	102	61.96	30.92	96.94 ± 0.10	20.37 ± 0.13	19.72 ± 0.13

While using 0.5 M  $\text{H}_3\text{PO}_4$ , as the supporting electrolyte did generally improve battery cycling behaviour, it also greatly reduced the solubility from 350 mM in 1 M HCl to only 140 mM in 0.5 M  $\text{H}_3\text{PO}_4$ . To combat this, a supporting electrolyte comprised of 0.5 M  $\text{H}_3\text{PO}_4$  and 0.5 M HCl was prepared. The solubility of **1** in this solution was increased to 347 mM, and in the same range as the maximum solubility achieved in 1 M HCl. Performance of the battery was assessed with 100 mM of **1** in this mixed salt electrolyte (Figure 10). Comparing the four electrolytes in Table 2, the mix of  $\text{H}_3\text{PO}_4$  and HCl yielded the best capacity retention with just over 100 cycles of significant capacity being achieved at a CE of 96.94% (after the first cycle) and a voltaic efficiency (VE) of 20.37%, reflecting the ratio of

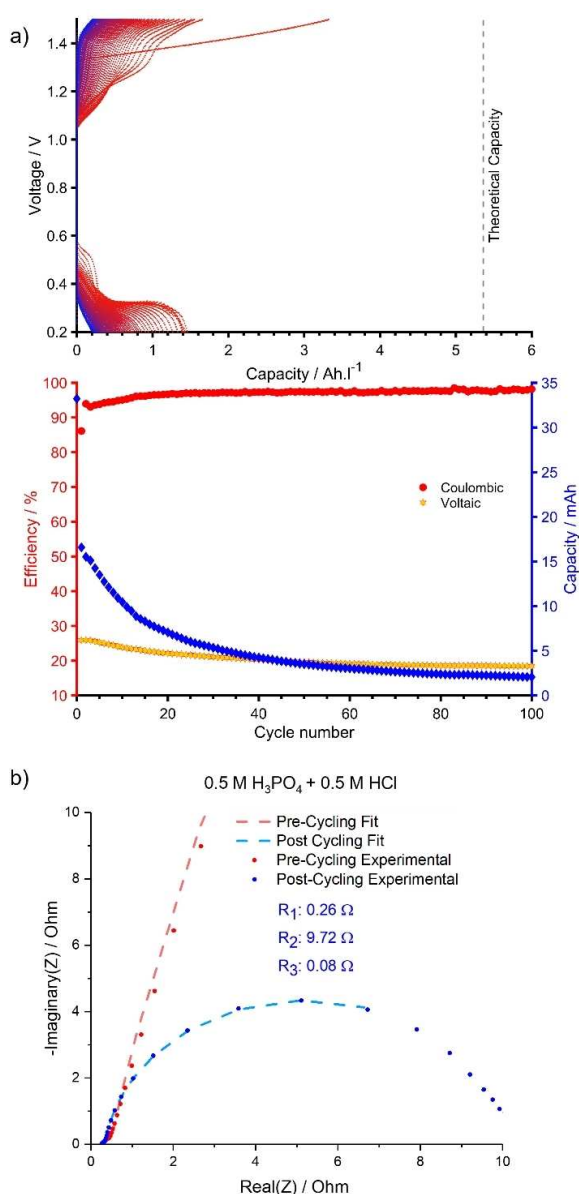


**Figure 10.** a) First 100 cycles of galvanostatic battery cycling for 100 mM **1** in 0.5 M  $\text{H}_3\text{PO}_4$  and 0.5 M HCl with a mixed  $\text{VCl}_2/\text{VCl}_3$  anolyte in excess. The full 200 cycles can be seen in Figure S14. The top is voltage vs. capacity while the bottom is CE (red), capacity (blue), and VE (orange) vs. the cycle number. b) Impedance of the first 200 cycles.  $R_1$ ,  $R_2$  and  $R_3$  are defined in Figure 9b.

charge and discharge voltages. Moreover, the capacity fade between the 1<sup>st</sup> and 2<sup>nd</sup> cycles was minimised. Combined with the much-improved solubility, these results demonstrate that, of the conditions investigated, 0.5 M  $\text{H}_3\text{PO}_4$  with 0.5 M HCl was the optimal supporting electrolyte.

EIS also provides important insight into this improved performance (Figure 10). After 200 cycles, the interfacial resistances of  $R_2$  and  $R_3$  were 0.20 and 9.47  $\Omega$ , respectively. These values are comparable to those found in 1 M HCl after only 100 cycles, possibly reflecting the formation of smaller, more soluble, oligomers rather than extended polymer chains and further reinforcing the dramatic effect of electrolyte conditions in disrupting the polymer formation, and in turn the change in conductivity of the cell.

It is possible that poor charge transfer kinetics at the electrode surface are contributing to the performance seen, especially with respect to the VE. A potential direction to explore in future work on triaryl amines would be modification of the electrode surface to improve hydrophilicity and charge transfer rates.<sup>[4]</sup>

## Conclusions

This work is the first to explore the potential of a triaryl amines (TAA) framework for aqueous organic redox flow battery (AORFB) applications. Five derivatives incorporating amino substituents were explored and the relationship between electron-donating and -withdrawing groups on stability was identified. While TAAs remain a potential framework for further exploration in AORFBs, currently the biggest barrier is the risk of polymerisation, which results in the passivation of the electrodes and a dramatic reduction in capacity limiting the amount of energy the battery can generate as well as the battery lifetime. However, by exploring a wider range of functional groups beyond amino substituents, a more stable redox active compound may be identified. Additionally, this work focused exclusively on electrolyte conditions, optimising other components such as the electrodes may provide further improvements.

Most importantly, this work emphasises the impact of electrolyte conditions on electrochemical behaviour and activity. Simple changes to the electrolyte system such as changing the salt and varying the salt concentration had a significant effect on the performance of the battery. By varying the supporting electrolyte, it was possible to improve the maximum number of cycles from 16 to over 100, increase the Coulombic efficiency (CE) from 92.30 to 96.94% and access an additional 20% of the theoretical capacity without affecting solubility.

## Experimental Section

Synthesis of the triaryl amines was conducted using an aromatic substitution reaction. A 2:1 molar ratio of an appropriate phenyl amine and aryl halide was used as well as CsF. Hydrogenations of nitro groups utilised hydrazine while acetic acid was used to convert cyano groups to carboxylic acids. Finally, iodomethane was



used to methylate amine groups. Further details, including characterisation of compounds 1–5 can be found in the Supporting Information.

CV and impedance measurements were performed using a VSP potentiostat from Biologic, a glassy carbon working electrode and platinum counter electrode. For acidic solutions a Ag/AgCl reference electrode was used. Initial electrochemical analysis was performed using EC-lab. Additionally, plotting was done using MATLAB and Origin.

Battery cycling data was measured using a commercial cell from Scribner Associates, the details of which can be found in the Supporting Information. Potentiostatic cycling was used in all cases. Potentiostatic electrochemical impedance spectroscopy (PEIS) was performed before and after the cycling of each cell.

## X-Ray Crystallography

Deposition Number 2249741 (for 1), contains the supplementary crystallographic data for this paper. These data are provided free of charge by the joint Cambridge Crystallographic Data Centre and Fachinformationszentrum Karlsruhe Access Structures service.

## Acknowledgements

The authors (N.L.F and R.B.J) would like to acknowledge the funding contributions of Shell and the EPSRC via I-Case studentships (grants no. EP/V519662/1 and EP/R511870/1 respectively). T.I would like to thank the ERC advanced Investigator Grant for CPG (EC H2020 835073). Thank you to Zhen Wang from the University of Cambridge for measuring GPC, the Yusuf Hamied Department of Chemistry's mass spectrometry service for MS measurements and analysis and Dr Andrew Bond from the University of Cambridge for XRD measurement and analysis.

## Conflict of Interests

The authors declare no conflicts of interest.

## Data Availability Statement

The data that support the findings of this study are available in the supplementary material of this article.

**Keywords:** aqueous · organic · redox · flow · battery · electrochemistry · supporting electrolyte · redox chemistry · triarylamine

- [1] A. Clemente, R. Costa-Castelló, *Energies* **2020**, *13*, 1–31.
- [2] J. Noack, N. Roznyatovskaya, T. Herr, P. Fischer, *Angew. Chem. Int. Ed.* **2015**, *54*, 9776–9809; *Angew. Chem.* **2015**, *127*, 9912–9947.
- [3] J. Cao, J. Tian, J. Xu, Y. Wang, *Energy Fuels* **2020**, *34*, 13384–13411.
- [4] J. Xu, Y. Zhang, Z. Huang, C. Jia, S. Wang, *Energy Fuels* **2021**, *35*, 8617–8633.
- [5] B. Huskinson, M. P. Marshak, C. Suh, S. Er, M. R. Gerhardt, C. J. Galvin, X. Chen, A. Aspuru-Guzik, R. G. Gordon, M. J. Aziz, *Nature* **2014**, *505*, 195–198.
- [6] R. M. Darling, K. G. Gallagher, J. A. Kowalski, S. Ha, F. R. Brushett, *Energy Environ. Sci.* **2014**, *7*, 3459–3477.
- [7] E. W. Zhao, T. Liu, E. Jónsson, J. Lee, I. Temprano, R. B. Jethwa, A. Wang, H. Smith, J. Carretero-González, Q. Song, C. P. Grey, *Nature* **2020**, *579*, 224–228.
- [8] R. B. Jethwa, E. W. Zhao, R. N. Kerber, E. Jónsson, D. S. Wright, C. P. Grey, *J. Mater. Chem. A* **2021**, *9*, 15188–15198.
- [9] D. G. Kwabi, Y. Ji, M. J. Aziz, *Chem. Rev.* **2020**, *120*, 6467–6489.
- [10] W. Zhou, W. Liu, M. Qin, Z. Chen, J. Xu, J. Cao, J. Li, *RSC Adv.* **2020**, *10*, 21839–21844.
- [11] D. G. Kwabi, K. Lin, Y. Ji, E. F. Kerr, M. A. Goulet, D. De Porcellinis, D. P. Tabor, D. A. Pollack, A. Aspuru-Guzik, R. G. Gordon, M. J. Aziz, *Joule* **2018**, *2*, 1894–1906.
- [12] C. G. Armstrong, K. E. Toghill, *Electrochem. Commun.* **2018**, *91*, 19–24.
- [13] J. D. Milshtein, R. M. Darling, J. Drake, M. L. Perry, F. R. Brushett, *J. Electrochem. Soc.* **2017**, *164*, A3883–A3895.
- [14] A. Orita, M. G. Verde, M. Sakai, Y. S. Meng, *Nat. Commun.* **2016**, *7*, 1–8.
- [15] C. Zhang, Z. Niu, S. Peng, Y. Ding, L. Zhang, X. Guo, Y. Zhao, G. Yu, C. Zhang, S. Peng, Y. Ding, L. Zhang, X. Guo, G. Yu, Z. Niu, Y. Zhao, *Adv. Mater.* **2019**, *31*, 1901052.
- [16] Tohru Nishinaga, *Organic Redox Systems, Synthesis, Properties and Applications*, Wiley, **2016**.
- [17] J. Wang, K. Liu, L. Ma, X. Zhan, *Chem. Rev.* **2016**, *116*, 14675–14725.
- [18] E. I. Romadina, I. A. Volodin, K. J. Stevenson, P. A. Troshin, *J. Mater. Chem. A* **2021**, *9*, 8303–8307.
- [19] G. Kwon, K. Lee, J. Yoo, S. Lee, J. Kim, Y. Kim, J. E. Kwon, S. Y. Park, K. Kang, *Energy Storage Mater.* **2021**, *42*, 185–192.
- [20] X. Wang, W. Tang, K. P. Loh, *ACS Appl. Mater. Interfaces* **2021**, *4*, 3612–3621.
- [21] E. Moulin, J. J. Armao, N. Giuseppone, *Acc. Chem. Res.* **2019**, *52*, 975–983.
- [22] F. Picini, S. Schneider, O. Gavati, A. Vargas Jentszsch, J. Tan, M. Maaloum, J. M. Strub, S. Tokunaga, J. M. Lehn, E. Moulin, N. Giuseppone, *J. Am. Chem. Soc.* **2021**, *143*, 6498–6504.
- [23] E. Moulin, F. Niess, M. Maaloum, E. Buhler, I. Nyrkova, N. Giuseppone, *Angew. Chem. Int. Ed.* **2010**, *49*, 6974–6978; *Angew. Chem.* **2010**, *122*, 7128–7132.
- [24] C. Karunakaran, M. Balamurugan, *Electron Paramagnetic Resonance Spectroscopy*, Elsevier Inc., **2018**.
- [25] W. Schlemmer, P. Nothdurft, A. Petzold, G. Riess, P. Frühwirt, M. Schmallegger, G. Gescheidt-Demner, R. Fischer, S. A. Freunberger, W. Kern, S. Spirk, *Angew. Chem. Int. Ed.* **2020**, *59*, 22943–22946; *Angew. Chem.* **2020**, *132*, 23143–23146.
- [26] V. P. Calkins, V. P. Calkins, *J. Am. Chem. Soc.* **1947**, *69*, 384–388.
- [27] P. Maruthamuthu, P. Neta, *J. Phys. Chem.* **1978**, *82*, 710–713.
- [28] Y. Li, J. Bao, M. Skyllas-Kazacos, M. P. Akter, X. Zhang, J. Fletcher, *Appl. Energy* **2019**, *237*, 91–102.

Manuscript received: January 27, 2023  
 Revised manuscript received: March 18, 2023  
 Accepted manuscript online: March 27, 2023  
 Version of record online: May 9, 2023